High pressure Cr^{3+} R-line luminescence of zoisite and kyanite: A probe of octahedral site distortion

Earl F. O'Bannon III[1*] and Quentin Williams[2]

[1]Physics Division, Lawrence Livermore National Laboratory, Livermore, California 94550, USA
[2]Department of Earth and Planetary Sciences, University of California Santa Cruz, Santa Cruz, California 95064, USA
[*]Corresponding Author: obannon2@llnl.gov

Abstract

The Cr^{3+} luminescence spectra of zoisite and kyanite, two geologically important minerals, were studied up to 40 and 20 GPa, respectively, in various pressure media. Cr^{3+} substitutes into the octahedral aluminum sites in both minerals and the R-line luminescence is a particularly sensitive site-specific probe of the octahedral Al site. Unlike many previous studies where Cr^{3+} luminescence was utilized, both these minerals have multiple highly distorted octahedral sites resulting in very large splitting of their R-lines, ~300 cm^{-1} in zoisite and ~360 cm^{-1} in kyanite (for reference, ruby is 29 cm^{-1}). For zoisite, the R-line splitting increases as pressure increases and more than triples from its ambient value by 40 GPa, while the R-line splitting in kyanite from the M1 and M2 sites does not change when compressed in a Ne pressure medium up to 20 GPa. We do not observe evidence of any phase transitions in either zoisite or kyanite across the pressure range of these new luminescence measurements. We present some high-pressure luminescence results where kyanite was known to be bridged between the diamond anvils and show how these spectra illustrate the different effect of uniaxial relative to hydrostatic stress on luminescence spectra.

Key words: zoisite, kyanite, high-pressure, luminescence, diamond anvil cell

Introduction

Zoisite [$Ca_2Al_3(SiO_4)(Si_2O_7)O(OH)$] contains ~2.0 wt.% and is an important source and carrier of water in subduction zones (Dobrzhinetskaya and Green, 2007; Nicholls and Ringwood, 1973; Ono, 1998; Peacock, 1990). For comparison, kyanite [Al_2SiO_5] is a common accessory mineral in eclogites, and can be found both in subduction zones where certain crustal rocks are subducted, and as a breakdown product of aluminous phases (Ono, 1998). The stability field of zoisite in a basalt + H_2O system extends to ~3.1 GPa

at 650 °C (Forneris and Holloway, 2003; Forneris and Holloway, 2004). It has a slightly larger stability field in the CaO-Al_2O_3-SiO_2-H_2O (CASH) system, which ranges from 4.0 GPa at 500 °C to as high as 7.0 GPa at over 1000 °C (Poli and Schmidt, 1998; Schmidt and Poli, 1994); beyond these pressures it breaks down to lawsonite-bearing assemblages. Zoisite has been studied with X-ray and spectroscopic techniques up to 34 GPa at 300 K, and no phase transitions have been reported (Alvaro et al., 2012; Comodi and Zanazzi, 1997; Winkler et al., 1989; Xu et al., 2019), while kyanite has been found to decompose into stishovite and corundum between 5-15 GPa and 1200-1900 K (Ono et al., 2007) and between 14-17.5 GPa and 1272-2273 K (Schmidt et al., 1997). At room temperature, a number of studies of kyanite up to 20 GPa using powder and single crystal X-ray diffraction as well as Raman spectroscopy did not find evidence for any phase transitions (Comodi et al., 1997; Friedrich et al., 2004; Liu et al., 2009; Mernagh and Liu, 1991; Yagi et al., 1998; Yang et al., 1997). However, at pressures >30 GPa and temperatures > 2000 K, other phases of kyanite have been reported to be stable (Ahmed-Zaid and Madon, 1991; Friedrich et al., 2004). New high-pressure phases kyanite-II and kyanite-III have been reported from multi-anvil studies at 13 and 17 GPa, but at temperatures exceeding 2000 K (Zhou et al., 2021; Zhou et al., 2018). Recently, (Gao et al., 2020) compressed kyanite up to 18.6 GPa at room temperature using both Raman and infrared spectroscopy and report that a first order phase transition to kyanite-II (which is likely distinct from the high-pressure/high-temperature kyanite-II polymorph) occurs at 9.7 GPa. These results distinctly differ from previous room temperature, high pressure X-ray and spectroscopic studies on kyanite (Comodi et al., 1997; Friedrich et al., 2004; Liu et al., 2009; Mernagh and Liu, 1991; Yang et al., 1997). Thus, part of the motivation for examining kyanite using luminescence is to determine whether a different probe can resolve any possible phase transitions that may occur under pressure at 300 K in this material.

Cr^{3+} luminescence spectra in the red typically consist of intense relatively sharp emission bands, and in some cases a broad emission band. The sharp emission bands are commonly referred to as R-lines. These emission bands are associated with the spin-forbidden ^2E-$^4A_2$ transition, with the $^4A_2$ state being

51 the ground state and the ^2E state being split in non-cubic environments (Syassen, 2008). The broad
52 emission band is assigned to the spin-allowed $^4T_2$-$^4A_2$ transition. At high crystal field strengths (Burns,
53 1993; Tanabe and Sugano, 1954), the narrow band ^2E-$^4A_2$ emission dominates the spectrum. For low
54 crystal field strengths (Burns, 1993; Tanabe and Sugano, 1954), the generally broader $^4T_2$-$^4A_2$ emission
55 band may dominate the emission spectrum. Both sharp and broad emission bands are observed at
56 intermediate crystal field strengths. The Cr^{3+} luminescence of ruby (Al_2O_3:Cr) is well characterized at
57 ambient and high pressures and has been widely used as an *in situ* pressure calibrant for high pressure
58 experiments (Syassen, 2008). This is due to its sharp strong R-line luminescence, lack of high-pressure
59 phase transitions across a wide pressure and temperature range, and chemical inertness towards
60 commonly used pressure media (Syassen, 2008).

61 Until recently, only a small number of other geologic materials have had their Cr^{3+} luminescence
62 characterized under pressure. These materials were examined for many of the same reasons as ruby and
63 include alexandrite ($BeAl_2O_4$), MgO, spinel ($MgAl_2O_4$) and a range of garnets (Chopelas and Nicol, 1982;
64 Jahren et al., 1992; Jovanic, 2000; Kottke and Williams, 1983; Wamsley and Bray, 1994). Cr^{3+} typically
65 substitutes into the Al^{3+} site and, since it has a slightly larger ionic radius than Al^{3+}, local site distortions
66 can arise from this substitution. Most of the previously minerals characterized by luminescence
67 spectroscopy under high pressures have only one or two unique Cr-bearing octahedral sites that are nearly
68 ideal or only slightly distorted. However, there are a large number of Cr^{3+} luminescence studies on more
69 crystallographically complex natural and synthetic materials at ambient pressure and various
70 temperatures (Gaft et al., 2015 and references therein).

71 Recently, there has been a growing interest in using Cr^{3+} luminescence as a site-specific probe in
72 geologic materials with moderate to highly distorted Cr-bearing octahedral sites, as well as lower
73 symmetry more chemically complex minerals (Hua et al., 2021; O'Bannon et al., 2018; O'Bannon and
74 Williams, 2016a; O'Bannon and Williams, 2016b; O'Bannon and Williams, 2017; O'Bannon and Williams,

2019). Moreover, due to the difference in ionic radius between Al and Cr, there can be extensive local distortion of the octahedral sites in which Cr^{3+} substitutes that cannot readily be characterized with techniques such as X-ray diffraction. Here, we present new high-pressure Cr^{3+} luminescence results on zoisite up to 40 GPa and kyanite up to 16 GPa. These two minerals have multiple highly distorted Al-sites, and they have R-line splittings of > 300 cm^{-1} at ambient conditions: a separation far in excess of that of ruby (29 cm^{-1}) and other minerals examined to date by luminescence under compression. As such, the primary goals of this study include determining how luminescence from highly distorted sites is altered by compression, and the degree to which shifts in distortion can be monitored using luminescent spectra.

Methods

Trace element concentrations of the kyanite and zoisite samples were measured with a PhotonMachines Analyte 193H, which is a 193-nm ArF excimer laser system coupled with a ThermoScientific ElementXR single-collect or magnetic sector ICP-MS. The instrument was calibrated with a SRM 610 trace element glass from NIST, and Al was used as the internal standard. All reported concentrations are in ppm and are an average from 4 measurements from different locations on the sample, and the standard deviation of the 4 measurements produces the reported uncertainties. The zoisite sample is from the Mundarara Mine, Arusha Region, Tanzania. The following trace elements were measured: Cr 4860 ± 2104, V 51 ± 22, Mn 91 ± 38, and Fe 6464 ± 2763 ppm; the variability is indicative of some possible compositional zoning within the sample. The kyanite sample is a typical light blue kyanite from an unknown locality which was selected for its strong R-line luminescence and low intensity broad band emission. The following trace elements were measured: Cr 2 ± 1, V 32 ± 2, Fe 194 ± 9 ppm, Mn below detection limit. Our utilization of natural samples is unlikely to produce markedly different local deformations associated with Cr-substitution than are present in synthetic samples: the overarching shift in

lattice parameters associated with Cr-substitution is quite linear from low Cr-concentrations to nearly 60 mol% Cr_2SiO_5 substitution in Cr-kyanites (Hejny et al., 2019). While no comparable data are available for zoisite, clinozoisite appears to show similarly linear lattice parameter trends with Cr-substitution (Nagashima et al., 2009).

High static pressures were generated with either Merrill-Bassett type diamond anvil cells (DACs) (Merrill and Bassett, 1974), symmetric piston-cylinder type DACS, or LLNL type membrane DACs (Jenei et al., 2013). They were equipped with 16 sided type Ia diamond anvils with culets ranging from 500 to 200 µm in diameter; the gasket material was either stainless steel, spring steel, or rhenium, and the pressure transmitting medium (PTM) was either methanol:ethanol (4:1), Ne, or He, depending on the particular experiment's target pressure. Single crystals of the sample were loaded in the sample chamber with a ruby sphere (Chervin et al., 2001) which was used for pressure calibration using well-known calibrations (Dewaele et al., 2008; Mao et al., 1986). The sample and the ruby were well separated so that luminescence spectra could be collected from the sample with no contamination from ruby luminescence. Ambient pressure low temperature measurements were carried out for peak assignment purposes, with the samples submerged in liquid nitrogen.

Luminescence spectra were collected either using a Horiba LabRAM HR Evolution Raman spectrometer, or a Princeton instruments SP-2500 spectrometer. For the measurements on the Horiba spectrometer, spectra were collected from 650-800 nm (15380-12500 cm^{-1}). The spectrometer focal length of this system is 800 mm. An Olympus BXFM-ILHS microscope with a 50x long working distance objective was used to focus the 532 nm laser beam onto the sample. An 1800 lines/mm grating with a corresponding spectral resolution of ~1 cm^{-1} (or, equivalently, ~0.05 nm) was utilized. For measurements on the Princeton Instruments spectrometer, luminescence spectra were collected from 680-770 nm. The spectrometer focal length of this system is 500 mm. A long working distance 30X Mitutoyo objective was used to focus the 488 nm laser beam onto the sample. A 1200 lines/mm grating with a corresponding

spectral resolution of ~1.14 cm^{-1} was utilized. Combinations of Gaussian and Lorentzian functions were fit to the luminescence spectra with either Horiba Labspec6 software or OriginPro software.

Results and Discussion

Zoisite

Zoisite is orthorhombic, so it is not considered a member of the epidote-group (Armbruster et al., 2006; Mills et al., 2009). It is a sorosilicate with mixed SiO_4 and Si_2O_7 groups and is found in metamorphic and pegmatitic rocks. Zoisite was originally named saualpite for the Saualpe locality in Carinthia, Austria where it occurs in eclogites. The first structural model of zoisite was proposed by Ito (1950). This structural model was later confirmed by Fresenko et al. (1955), Dollase (1968), and Ghose and Tsang (1971). Zoisite has one octahedral chain parallel to [010] with two edge-sharing Al octahedra M1,2 (sometimes referred to as M1) and M3 (sometimes referred to as M2). The two metal sites have very different distortions (Figure 1), which can be quantified by calculating the quadratic elongation (QE) and angle variance (AV) described by Robinson et al. (1971). The QE of M1,2 is 1.006 and for M3 it is 1.021, while the AV is 19.4 for M1,2 and 46.4 for M3 using the single-crystal data from Alvaro et al. (2012). These chains are linked by isolated SiO_4 tetrahedra T3 and Si_2O_7 groups T1 and T2, and in between the octahedral chains and the silica tetrahedra are two crystallographically unique 7-fold sites that are occupied by Ca. The hydrogen atom is bonded to O10 of the octahedral chain and hydrogen bonded across to the O4 atom of the adjacent octahedral chain. Neutron diffraction of zoisite has confirmed the configuration of the hydroxyl unit (Camara et al., 2012; Smith et al., 1987).

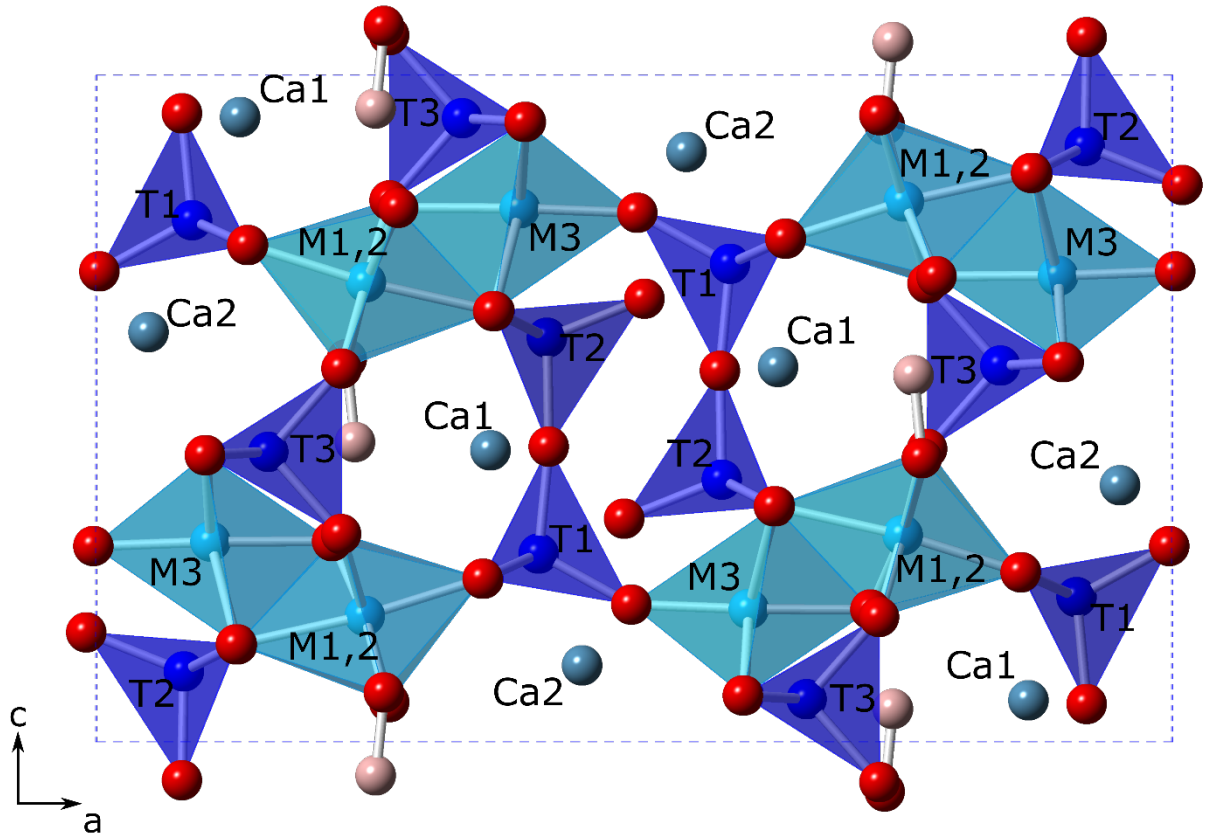

Figure 1. Crystal structure of zoisite showing the isolated SiO_4 site T3 and the Si_2O_7 sites T1 and T2, as well as the two octahedral sites M1,2 and M3, with M3 being highly distorted. Crystal structure diagram generated in CrystalMaker®.

Our 298 and 77 K spectra (Figure 2) are in good agreement with the spectra of a natural Tanzanian zoisite reported by Koziarska et al. (1994). At 77 K, the R_1 peak shifts to 708.6 nm from its 298 K location of 709.3 nm, and we observe a complete quenching of the R_2 peak that is observed at 691.9 nm in our 298 K spectrum. Additionally, several sharp bands that are likely associated with R-line emission from the less distorted M1,2 site are also observed. In particular, there is a relatively intense and sharp emission band that becomes resolvable at 77 K which could be an R-line from V^{2+} emission (Inset Figure 2). Vibronic features and/or paired emission bands (N-Lines) that contribute to the broad, distributed emission on the higher wavelength side of the

155 R_1 peak are also quenched at 77 K. The relatively high temperature at which we observe
156 quenching of R_2 can be explained by the large R-line splitting in zoisite. The temperature range
157 over which R_2 quenches scales exponentially with an activation energy that is roughly the R_1-R_2
158 separation, obeying the Arrhenius formula (Weinstein, 1986). Speculatively, there are two
159 emission bands (labelled by tick marks in the inset of Figure 2) which could be the R-lines
160 associated with the less distorted M1,2 site. If this were the case, the R-line separation for the R-
161 lines from this site at 77 K is ~115 cm^{-1}, which would be larger than the expected splitting at room
162 temperature. However, the distortion of the M1,2 site in zoisite (Alvaro et al., 2012) is less than
163 the distortion of the M1 site in spodumene (Arlt and Angel, 2000), while this possible R-line
164 separation in zoisite is greater than observed in spodumene at 77 K, which is 90.2 cm^{-1} (O'Bannon
165 and Williams, 2016b). Thus, the observed separation of these two emission bands is not fully
166 consistent with expectations given the distortion of the site. Nevertheless, the volume of the
167 M1,2 site is compatible with the observed emission peak positions. Therefore, luminescence
168 lifetime measurements would likely be needed to unambiguously distinguish whether these
169 emission bands are Cr^{3+} R-lines. The possible emission band from V^{2+} near 714 nm that is
170 observed at 77 K is difficult to consistently resolve across the pressure range of these
171 measurements, but it appears to shift like the Cr^{3+} R_1 emission band, and its relative intensity also
172 increases under compression.

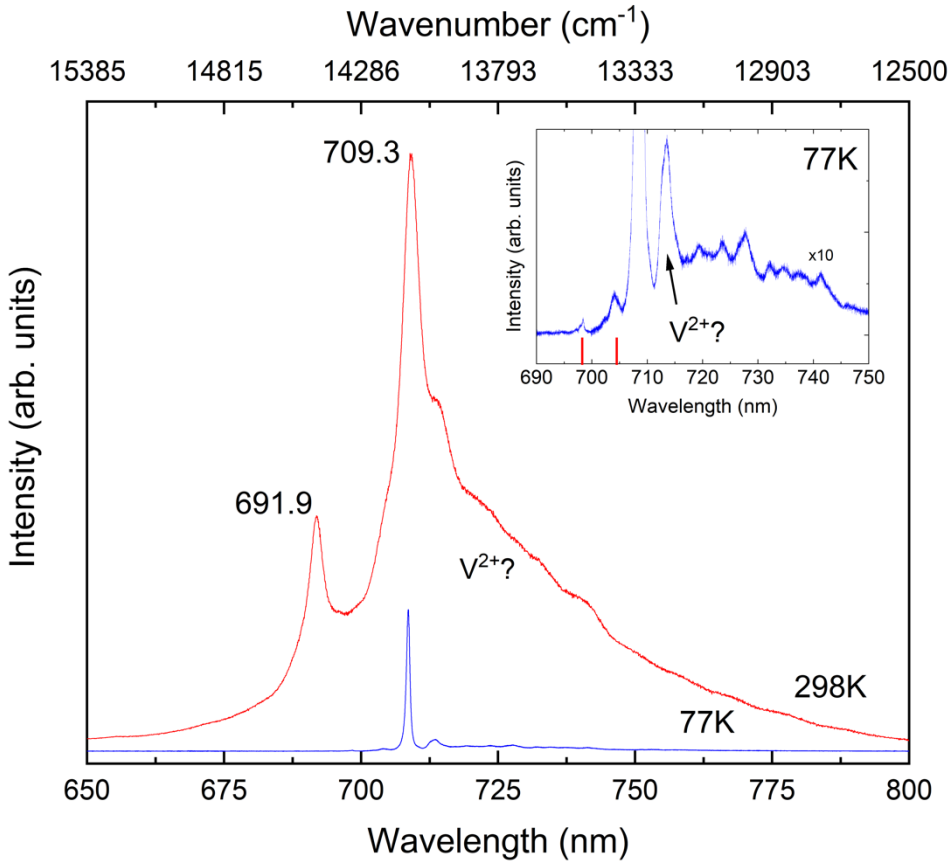

Figure 2. Representative Cr^{3+} luminescence spectra of zoisite at 298 K and 77 K. The inset shows a zoom-in of the 77 K spectrum (~x10), and the vertical lines in the inset mark the possible positions of R-lines originating from the M1,2 site. Possible emission from V^{2+} is also labelled in the inset.

Representative high-pressure Cr^{3+} luminescence spectra are shown in Figure 3. Three runs were conducted in three different pressure media (4:1 methanol:ethanol, Ne, and He) to a maximum pressure of 40 GPa. We fit one peak under each R-line, while the broad emission band is more difficult to deconvolve since it may be partly due to Cr^{3+}, V^{2+} and/or Fe (Koziarska et al., 1994). Since the splitting of the ^2E state is produced by deviations from ideal octahedral symmetry, R-line separation is regarded as an indicator of the degree of octahedral distortion. Ruby has an Al-site that is close to an ideal octahedron and has an R-line splitting of ~29 cm^{-1} (Syassen, 2008). The octahedral sites M1,2 and M3 in zoisite are, in comparison, highly distorted

(Figure 1) and zoisite has an R-line separation of ~340 cm^{-1} (Koziarska et al., 1994). M3 is the more distorted octahedral site in zoisite, so given both the size of the observed splitting and its larger size, it is probable that Cr^{3+} preferentially substitutes into the M3 site over the M1,2 site. This perhaps simplified idea of larger transition-metal cations substituting into the larger, more distorted site is supported by single-crystal X-ray diffraction (Dollase, 1968; Dollase, 1969; Dollase, 1971; Grapes, 1981), Mössbauer spectroscopy (Dollase, 1973), and previous ambient-pressure luminescence spectra (Koziarska et al., 1994) of transition-metal bearing zoisite and zoisite-related phases. The diffraction and Mössbauer studies on a suite of closely related minerals (allanite, epidote, hancockite, piemontite) show that larger cations preferentially substitute into the larger more distorted M3 site, although some substitution into the M1,2 site is also observed. The room temperature luminescence spectrum has strong broad band luminescence (Figure 2), which would likely obscure any low intensity sharp line emission from minor levels of substitution in the less distorted M1,2 site. Yet, it is highly likely that the majority of the Cr^{3+} that has substituted into the zoisite structure (and from which we observe emission) is in the M3 site.

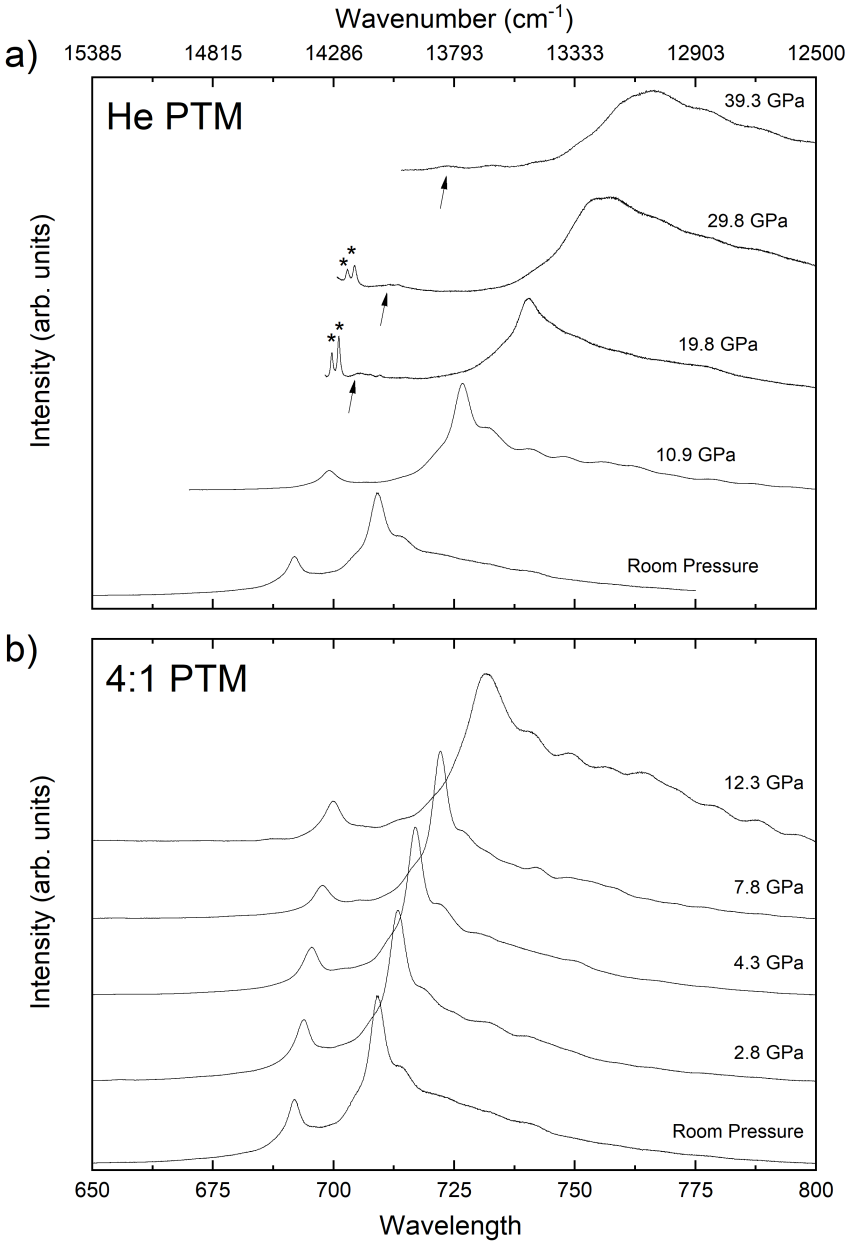

Figure 3. Representative high-pressure luminescence spectra of zoisite (a) He pressure medium and (b) 4:1 methanol ethanol pressure medium. In the He run, ruby emission from the pressure calibrant was also observed in our spectra; these are marked with asterisks, and the arrow indicates the position of the R_2 band of zoisite.

R-line positions as a function of pressure are shown in Figure 4. There is no evidence of a high-pressure phase transition within this pressure range, which is consistent with recent single-crystal X-ray diffraction results (Xu et al., 2019). The decompression data show that the changes

211 that occur on compression are fully reversible with no hysteresis. At ambient conditions, the
212 wavelengths of emission associated with R_1 and R_2 are 709.3 and 691.9 nm. The pressure shift
213 from the He run of R_1 is -27.2(3) cm^{-1}/GPa, while for R_2 it is -12.5(1) cm^{-1}/GPa; these were
214 determined by non-weighted linear fits. The R_1 shift is the largest known pressure shift of Cr^{3+} R-
215 lines in an oxide reported to date. This is most straightforwardly understood in terms of the
216 compressibility of the M3 site in zoisite. The M3 site in zoisite is more compressible than the
217 octahedral sites in most other minerals in which Cr^{3+} substitutes for Al^{3+} (Alvaro et al., 2012), such
218 as spodumene (Arlt and Angel, 2000), ruby (d'Amour et al., 1978; Finger and Hazen, 1978),
219 clinochlore (Welch and Marshall, 2001), and beryl (Hazen et al., 1986). Because of the differing
220 pressure shifts of R_1 and R_2, the initially large R-line separation increases even more as pressure
221 increases, and by ~40 GPa the R-line separation has nearly tripled from its ambient pressure value
222 (Figure 5). Single-crystal X-ray diffraction of zoisite up to 8 GPa confirms that the M3 site becomes
223 more distorted on compression, as manifested by the AV and QE of the M3 site (Alvaro et al.,
224 2012), and our luminescence data indicate that this trend continues to at least 40 GPa.

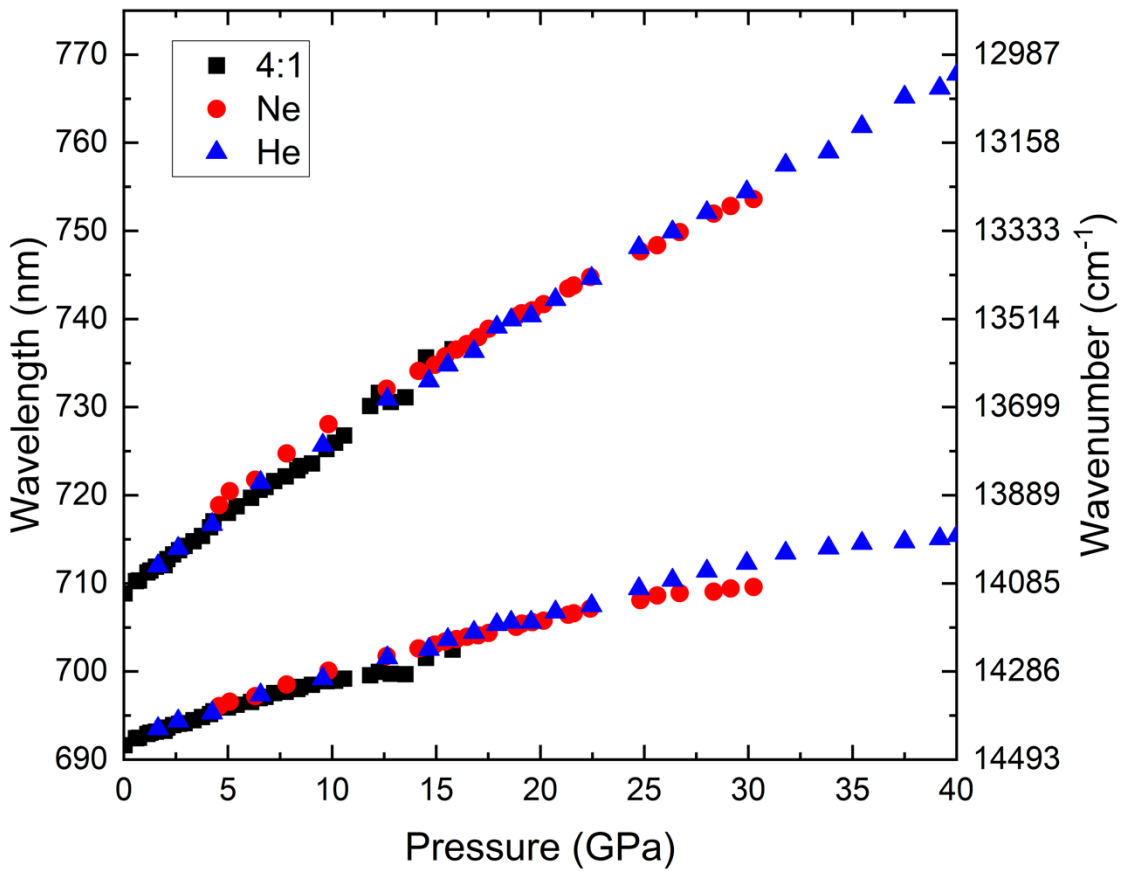

Figure 4. (a) R_1 and R_2 peak positions of zoisite as a function of pressure from three separate runs using different PTM. Error bars are smaller than the symbols.

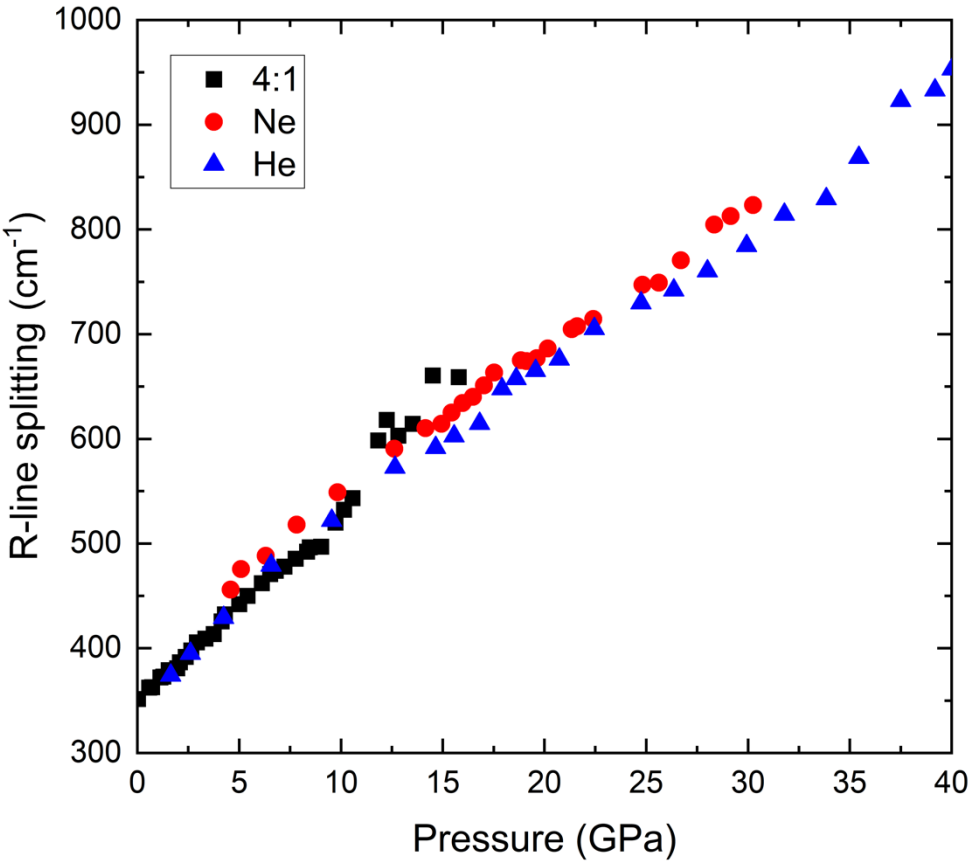

Figure 5. R-line splitting as a function of pressure. Note that the R-line separation nearly triples from its ambient value by 40 GPa. The slight differences in R-line separation between different runs is likely due to the different pressure media that were used. Note the increased scatter above ~10 GPa in the 4:1 methanol:ethanol data.

The results of different PTM are primarily manifested in the R_2 peak positions where changes in slope occur at ~25 GPa in Ne and ~32 GPa in He. It is possible that these changes in slope are indicators of the onset of non-hydrostatic conditions. However, it has been reported that the pressure shift of R_2 in ruby is independent of crystal orientation and non-hydrostatic stresses (Chai and Brown, 1996; Gupta and Shen, 1991), and R_2 may provide a more reliable indicator of the local mean stress. Moreover, the standard deviation in pressure in a He medium at 32 GPa is ~0.15 GPa, while it is ~0.22 GPa in Ne at 25 GPa (Klotz et al., 2009), so these changes in slope may not be occurring at the same differential stress. It is possible that the change in slope

of R_2 is evidence of a change in local compressional mechanism, and/or perhaps be indicative of precursory behavior to a phase transition at pressures > 40 GPa. The intensity of R_2 also decreases dramatically under compression, which increases our uncertainties in the peak position of R_2 above ~20 GPa. This decrease in intensity is certainly generated by the increase in R-line separation shown in Figure 5: the amplitude of R_2 relative to R_1 is in accord with Boltzmann's law (e.g., Koziarska et al., 1994), and the increased separation thus suppresses the R_2 amplitude. The anticipated reduction in intensity of R_2 at constant temperature for the factor of 3 increase in splitting across the pressure range of our measurements is about a factor of 20, which is in approximate accord with our observations (Figure 3a).

The broad band emission to the longer wavelength side of the R-lines is more difficult to assign to a particular dopant. This extended, relatively featureless emission shifts to longer wavelengths, and its relative intensity and its width increase at higher pressures (although it is difficult to fit accurately). This broad band emission occurs at wavelengths that are consistent with the Cr^{3+} $^4T_2$ -> $^4A_2$ transition. It has also been suggested that this broad band emission is due to V^{2+} (Koziarska et al., 1994). Since Cr^{3+} and V^{2+} both have a d^3 configuration, their luminescence spectra are quite similar. The main differences lie in intensity, wavelength, and lifetime of emission associated with these transition metals. This broad band is likely the $^4T_2$ transition from either Cr^{3+} and/or V^{2+} (although there may also be a vibronic component within the broad band), and it shifts to longer wavelength under compression and persists to the highest pressures of this study, suggesting that the crystal field strength remains weak to intermediate across the pressure range of these measurements. In order to unambiguously assign this broad band emission to Cr^{3+} or V^{2+} or both is not possible from steady state luminescent excitation, as lifetime measurements

would be needed.

Kyanite

Kyanite is one of the three Al_2SiO_5 polymorphs found in crustal and upper mantle assemblages, with the other two being sillimanite and andalusite. The pressure-temperature range where these polymorphs are stable span the conditions of regional metamorphism. These polymorphs are important index minerals used in metamorphic petrology to estimate the *P-T* conditions of rocks. The crystal structure of kyanite was first described by Naray-Szabo et al. (1929) and later by Burnham (1963) who used single-crystal X-ray diffraction. Kyanite is the high-pressure, low temperature polymorph, which has four unique octahedral Al sites and two unique tetrahedral Si sites (Figure 6). There are two groups of octahedra, the chain octahedra (M1 and M2) and the chain-connecting octahedra (M3 and M4). The most distorted metal site (based on the QE and AV) is M3, followed by M2 and M1 which have very similar distortion parameters, and the least distorted and smallest volume site is M4, using ambient single-crystal data from Comodi et al. (1997).

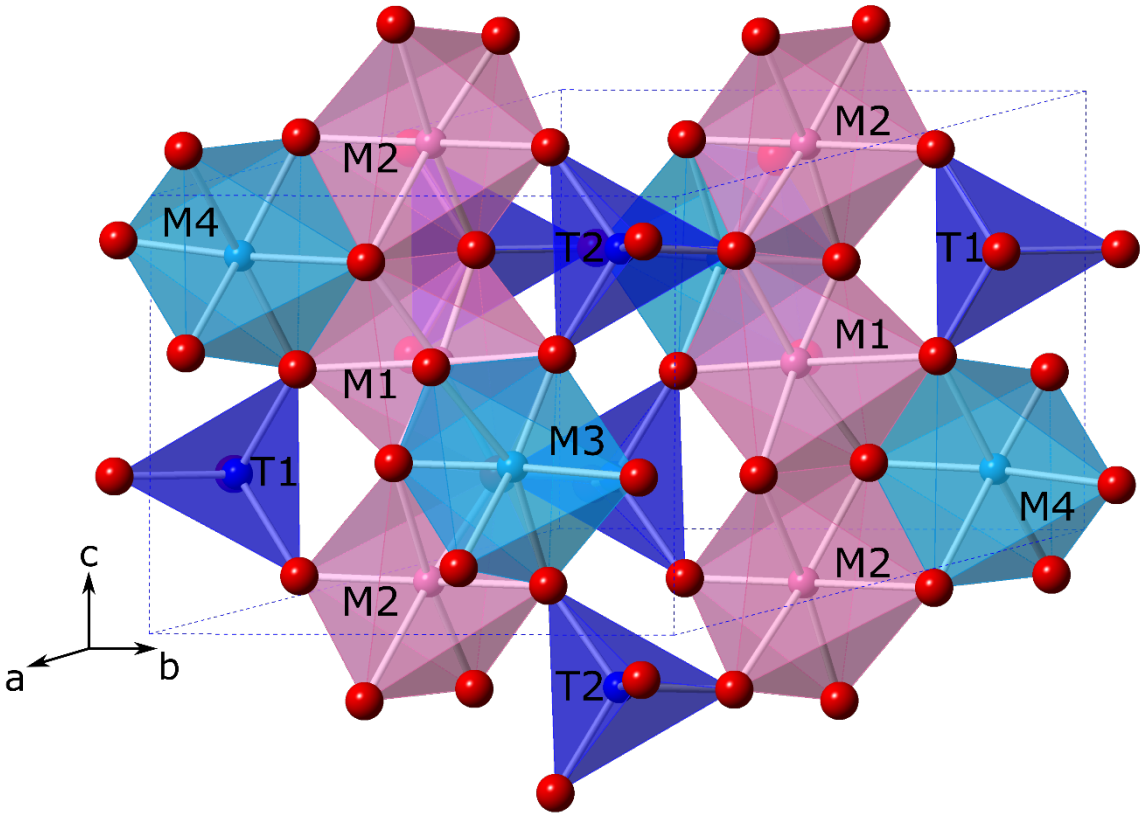

Figure 6. Crystal structure of kyanite. The chain octahedra are M1 and M2 and the chain connecting octahedra are M3 and M4. The two tetrahedral sites are also shown as T1 and T2. Crystal structure diagram generated in CrystalMaker®.

Ambient pressure luminescence spectra collected at 298 and 77 K are in good agreement with previously reported spectra collected at 300 and 26 K (Wojtowicz, 1991), at room temperature and 77 K (Platonov et al., 1998), and at 16 K (Czaja et al., 1995). Our spectra are shown in Figure 7; in order to resolve all of the features in the vicinity of the R-lines and the accompanying broad band emission, different laser powers and collection times were used. At 298 K, two emission bands can be easily deconvolved from each of the sharp emission lines. At 77 K, the two emission bands present at each of the 298 K sharp emission lines are clearly distinct and separated. The two higher intensity components (outer bands) originate from one Cr^{3+} site and are designated R_1 and R_2, while the two lower intensity components (the inner emission bands) likely originate from a different Cr^{3+} site and are named R_1' and

294 R_2'. At 298 K the deconvolved peak positions for R_1 and R_2 are 705.9 and 688.5 nm, while for R_1' and R_2'
295 they are 704.7 and 690.3 nm. At 77 K, the R_1 and R_2 bands shift to 704.9 and 687.5 nm while R_1' and R_2'
296 shift to 703.4 and 689.3 nm.

297 Notably, the measured Cr^{3+} concentration in our kyanite sample is lower than the measured V^{2+}
298 concentration, so it is possible that V^{2+} emission is also observed in our luminescence spectra. Our LA-
299 ICPMS results indicate that the trace element distribution was not homogeneous and that our kyanite
300 sample was chemically zoned. We selected samples that were close to the location where the LA-ICPMS
301 analysis was performed but, given the zonation, it is likely that the samples that were loaded into the DAC
302 had trace element concentrations that differed from the ICPMS analysis spot. However, it has been
303 reported that the Cr concentration in natural kyanite samples with strong narrow emission bands can be
304 very low, with emission observed from samples with less than 0.001 Cr^{3+} per formula unit (Platonov et al.
305 1998; Gaft et al. 2015). Thus, the quantum efficiency of Cr^{3+} emission in kyanite is likely quite high, in
306 accord with the assumptions of Wojtowicz (1991). The wavelength of the emission bands we observe at
307 both 77 K and 298 K under steady state excitation agree well with previous time resolved luminescence
308 measurements reported by Gaft et al. (2015). Gaft et al. (2015) report that the decay times of the emission
309 bands are consistent with emission from Cr^{3+}. Therefore, in accord with Gaft et al. (2015), all of our
310 assignments assume that Cr^{3+} is the luminescing species responsible for the observed emission bands. We
311 do note, as did Gaft et al. (2015), that a detailed investigation of synthetic kyanites with different Cr and
312 V concentrations is still needed to fully characterize if emission bands from V^{2+} are observed in kyanite.

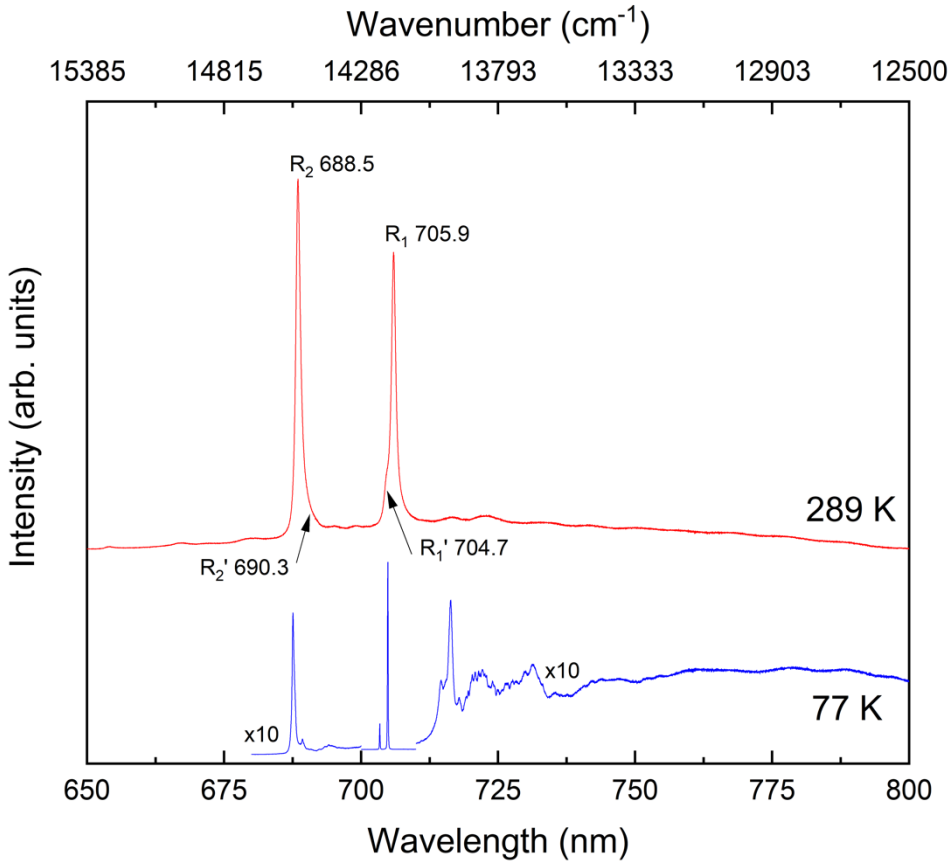

Figure 7. Representative steady state Cr^{3+} luminescence spectra of kyanite 298 K and 77 K. Note that the R_2 emission bands are not entirely quenched in the 77 K spectrum.

Previous assignments of the emission bands have not been straightforward; as discussed above, kyanite has four unique octahedral sites (Figure 6), the chain octahedra (M1 and M2) and the chain-connecting octahedra (M3 and M4). Langer and Seifert (1971) noted that from a geometric point of view, there is no reason why Cr^{3+} would prefer one group of sites over the other. However, based on a comparison between observed quotients of structure factors to those calculated from different models of Cr^{3+} distribution, the best agreement is found when Cr^{3+} does not occupy the M4 site (Langer and Seifert, 1971). Wojtowicz (1991) examined Cr-kyanite using a combination of absorption, steady state, time resolved, and luminescence decay measurements and found that Cr^{3+} emission is observed from 3 of the 4 octahedral sites, with M4 being "dark." Wojtowicz (1991) proposed that the M4 site could contain Cr^{3+} but that the center might be dark (non-emitting) if the Bartram-Stoneham criterion is fulfilled

(Bartram and Stoneham, 1975). However, Wojtowicz (1991) found that the Bartram-Stoneham criterion was not fulfilled for the M4 site and note that the larger Cr^{3+} ion may not substitute easily into the highest field site (smallest volume site). For comparison, Yeung et al. (1994) conducted a crystal field analysis of the kyanite absorption, emission and excitation spectra and concluded that substitution of Cr^{3+} into the M4 site was unlikely. Three magnetically inequivalent sites were identified in kyanite using electron paramagnetic resonance spectroscopy (Hutton and Troup, 1964), again supporting the presence of one unoccupied site. From a simple crystal structure perspective, M4 is not only the smallest volume site but also the least distorted site (QE = 1.013 and AV = 41.9) meaning Cr^{3+} would be more likely to substitute into the other sites first.

Our 77 K spectrum offers additional insight into the nature of the emission bands near 688 nm. At 26 K, Wojtowicz (1991) did not observe these emission bands: they were quenched to the degree that they were not resolved, and they are quite low amplitude (yet resolved) in the spectrum at 16 K of Czaja et al. (1995). At 77 K, they are clearly observed, which is strong evidence that these emission bands can be assigned as the R_2 component of the split ^2E emission band. The site nomenclature previously used by different authors in the spectroscopic literature is inconsistent; we use the mineralogically accepted site nomenclature M1-M4 for the four unique octahedral sites in kyanite. Our assignments are based on (1) site volumes, (2) site distortions, (3) intensity of the emission bands, and (4) the assumption that Cr^{3+} does not substitute into the M4 site. We assign the lower wavelength peak near 688 nm and the higher wavelength peak near 705 nm (the strong outer bands in Figure 7) to R_2 and R_1 originating from the M1 site; this is in accord with the preferred assignment of Yeung et al. (1994). The higher wavelength peak near 688 nm and the lower wavelength peak near 705 nm to R_2' and R_1' are assigned as being associated with the M2 site (See figure 7). That the QE of M1 and M2 are identical (M1 and M2 QE = 1.016) and their angle variance is similar (M1 AV = 47.7 and M2 AV = 50.8), coupled with the locations and splittings of the two sets of bands being generally similar, provides support for our assignments. These assignments are

also in accord with those of the absorption spectrum of blue Tanzanian kyanite of Wildner et al. (2013). The interpretation that the splitting of the emission bands is derived from Cr occupancy within two sites, while in accord with the assignments of Yeung et al. (1994), Czaja et al. (1995), Wojtowicz (1991) and Wildner et al. (2013), is at odds with that of Platonov et al. (1998), who attributed the splitting to a superposition of kyanite emission and emission from a corundum-type exsolving solid solution. Notably, the substitutional behavior of Cr in kyanite may shift at very high Cr contents: in synthetic samples with more than a 1:1 Cr/Al ratio, Hejny et al. (2019) observed a preference of Cr for the M3 site. Within more dilute, natural abundance samples (and perhaps within more dilute synthetic samples: Langer and Seifert, 1971), the spectroscopic consensus is that Cr substitution into the M1 and M2 sites predominates. Thus, while emission from Cr-substitution in M1 and M2 clearly dominate the spectrum, there may be evidence of Cr^{3+} emission from the M3 site manifested as the $^4T_2$ emission band (in the 77 K spectrum): a broad feature centered near 770 nm (Czaja et al., 1995), indicating a weaker crystal field at this site. This is in line with crystal structure data which show that M3 is both the largest metal site and the most distorted (QE= 1.019 and AV= 58.0). However, attempts to follow this broad emission band under pressure were unsuccessful.

We observed differences in the luminescence spectra with different orientations of the sample with respect to the polarization direction of the laser excitation. Our kyanite sample displayed the typical elongated columnar crystal habit, which was easily seen in the small single crystals that were cut from the main specimen. Therefore, the *a*-axis was commonly parallel to the incident laser during our measurements and the *b*-*c* plane was perpendicular to the laser probe. In our ambient measurements, the R_1 peak intensity was lower than the R_2 peak intensity when the *c*-axis was perpendicular to the polarization direction of the laser beam. When the *c*-axis was parallel to the polarization direction of the laser, the R_1 peak intensities were greater than the R_2 peak intensities (Figure 8). These differences in the Cr^{3+} luminescence spectra are most likely connected with the different distortions/orientations of the M1

and M2 sites which alternate along the *c*-axis oriented chains. Gaft et al. (2013c & 2015) also noted this polarization behavior in gem quality greenish kyanite and reported the same change in the relative intensities of R_1 and R_2 with different crystallographic orientations relative to the polarized laser probe. They suggest that the luminescence lines with long decay times are polarized in different directions. During our high-pressure measurements, spectra were collected in both orientations at each pressure step.

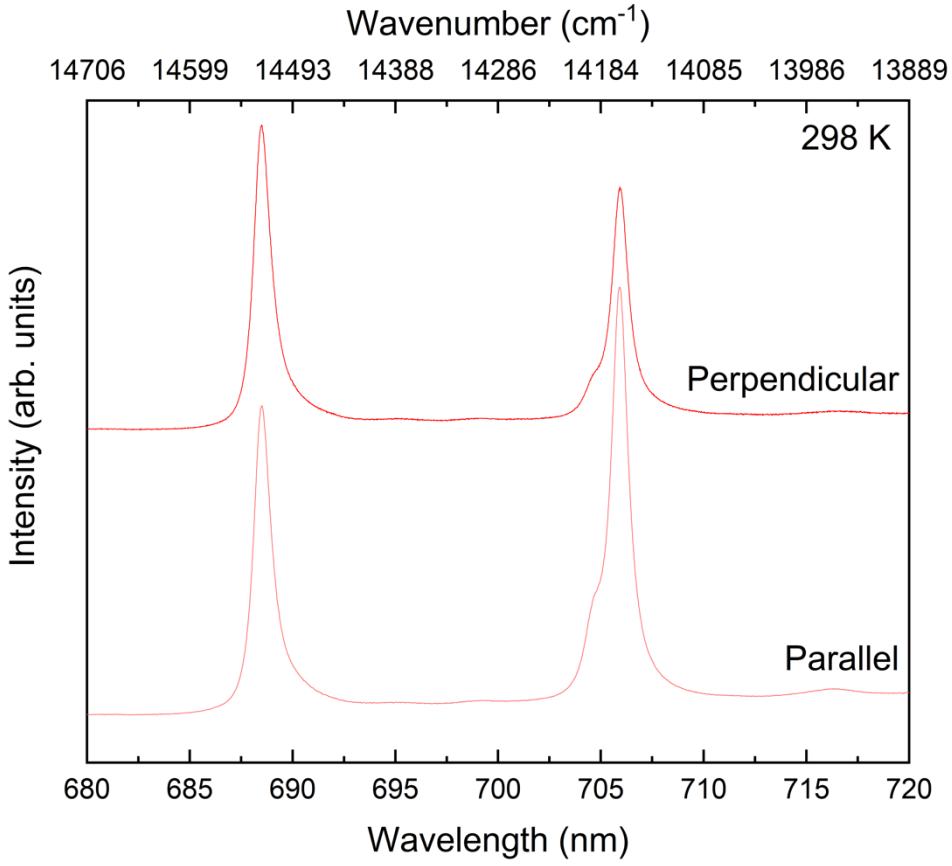

Figure 8. Steady state luminescence spectra of kyanite at ambient conditions showing changes in relative intensities with the *c*-axis of the sample both perpendicular and parallel to the polarization direction of the laser excitation.

Representative high pressure luminescence spectra from the parallel orientation compressed in both a Ne and 4:1 PTM are shown in Figure 9. There are no major differences (beyond relative band intensities and peak widths) in the luminescence spectra, or their pressure dependence, between the two runs in different PTM. In the 4:1 PTM run we collected spectra with the *c*-axis both parallel and

perpendicular to the laser polarization up to a maximum pressure of ~17 GPa. When the c-axis is parallel to the polarization direction of the laser, the two sets of emission bands become well separated above ~1 GPa and can easily be tracked visually. For the perpendicular orientation (not shown), the R_2' component is more difficult to visually track but can be deconvolved across the entire pressure range of these measurements. Attempts to deconvolve the broad, longer wavelength $^4T_2$ emission bands associated with both the M1 and M2 sites and possibly the M3 site were unsuccessful. The full width at half maximum (FWHM) of R_1 at ambient conditions is ~25 cm^{-1} and in the 4:1 run it remains essentially constant under compression up to ~10 GPa. Above this pressure, the FWHM of R_1 begins to increase, reaching ~46 cm^{-1} at ~16 GPa. In the Ne run, the FWHM of R_1 ranges from ~23-28 cm^{-1} across the entire pressure range, and no discontinuous changes or changes in slope are observed. This can be seen clearly in Figure 9 by comparing the spectra collected at ~16 GPa in the Ne and 4:1 PTM.

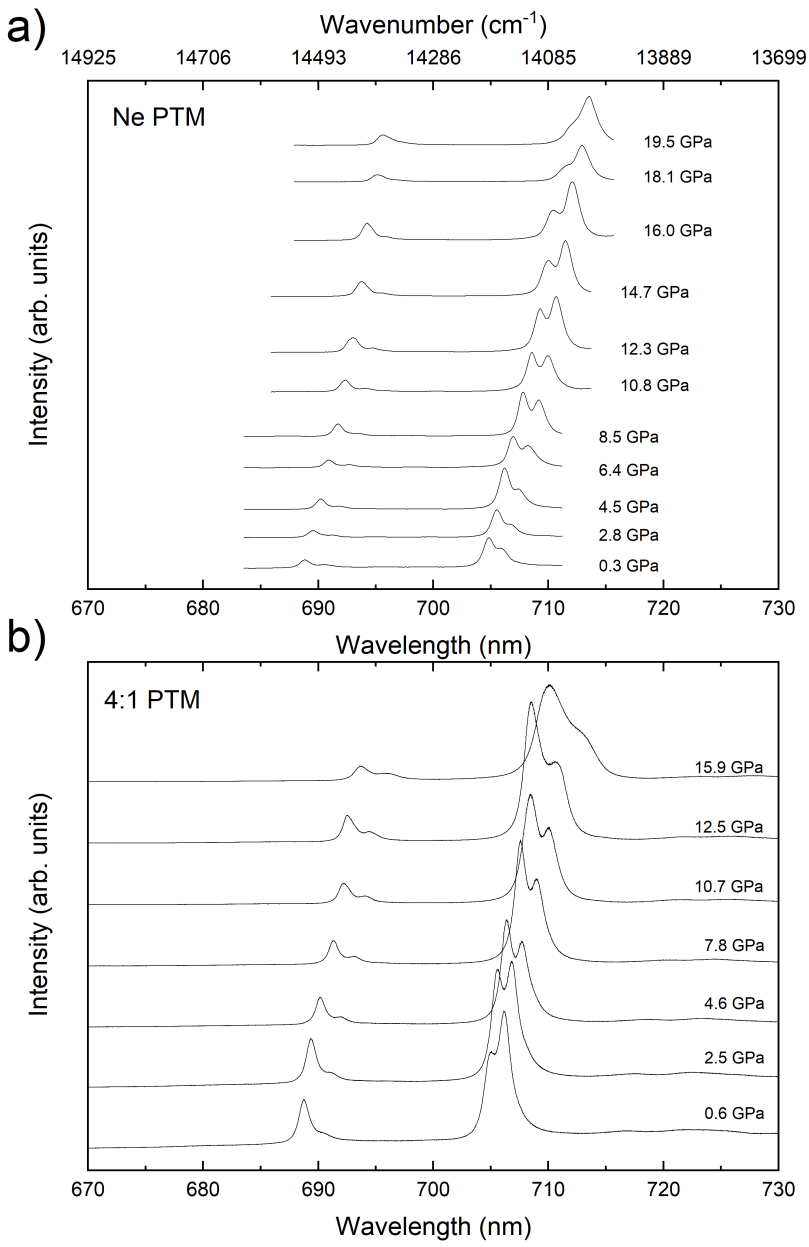

Figure 9. Representative high-pressure Cr^{3+} luminescence spectra of kyanite collected (a) in a Ne PTM with the *c*-axis roughly parallel to the laser polarization and (b) in a 4:1 PTM with the *c*-axis parallel to the laser polarization.

The pressure shift of the R-lines from both the M1 and M2 sites for the parallel orientation from the Ne and 4:1 PTM runs are shown in Figure 10. All the emission bands show a smooth increase in wavelength as pressure is increased, and no discontinuities or significant changes in the slope are observed up to 16 GPa. There is a slight dip in the trend of the R-lines above ~10 GPa in the 4:1 run, and

411 there may be a slight change in the slope above this pressure. In the Ne run, the R-lines shift essentially
412 linearly and no discontinuities or changes in slope are observed up to ~20 GPa. In the 4:1 run, the R-line
413 splitting from both the M1 and M2 sites remains essentially constant until about 10 GPa, where the
414 separation of the bands associated with the M1 site starts to increase, while it slightly decreases for those
415 generated by the M2 site (Figure 11). The sudden change in the R-line separation may be an indication of
416 a change in compression mechanism in which the M1 site becomes more distorted and the M2 site
417 becomes less distorted. However, in the run where a Ne PTM was used the R-line splitting for the M1 site
418 shows a very slight increase of 0.34(2) cm^{-1}/GPa (which was determined from a non-weighted linear fit)
419 while the R-line splitting for the M2 sites remains essentially constant up to ~20 GPa. It is likely that the
420 observed changes in the kyanite luminescence spectra from the 4:1 run are due to the onset of non-
421 hydrostatic conditions above ~10 GPa. It is well known that 4:1 methanol:ethanol undergoes a glass
422 transition at ~10.5 GPa and that pressure gradients form above this pressure (Klotz et al., 2009). Kyanite
423 appears to be particularly sensitive to the onset of non-hydrostatic conditions. It is clear from the high-
424 pressure run in a Ne PTM that the behavior observed above 10.5 GPa in the 4:1 run is anomalous. The
425 pressure shift of the R-lines as determined from non-weighted linear fits to the Ne data are R_1= -7.86(3)
426 cm^{-1}/GPa, R_1'= -7.67(4) cm^{-1}/GPa, R_2= -7.51(4) cm^{-1}/GPa, and R_2'= -7.59(5) cm^{-1}/GPa. The relative
427 constancy of the R-line separation under pressure is in general accord with previous single-crystal X-ray
428 results to 4.7 GPa that showed that the quadratic elongation of the M1 and M2 sites either remained
429 constant (Comodi et al., 1997) or weakly decreased under compression (Yang et al., 1997).

430 Notably, two prior studies conducted reconnaissance investigations of the pressure shift of the R_1
431 line(s) of kyanite to 14 GPa (Mernagh and Liu, 1991; Parthasarathy, 1997). Both studies tracked only the
432 R_1 emission under pressure. Mernagh and Liu (1991) report that above pressures of 5 GPa a single
433 emission band with a weak shoulder on the high frequency side is observed, while Parthasarathy (1997)
434 report that the two R-lines merge at ~6 GPa with a single broad fluorescence peak observed to 14 GPa.

Parthasarathy (1997) also misassigns the two emission bands near 705 nm as R_1 and R_2, which is inconsistent with this study and previous studies (Czaja et al., 1995; Wojtowicz, 1991). As discussed above and seen in Figure 9, the two R_1 components remain well separated across the entire pressure range of our new measurements when the *c*-axis of the sample is parallel or nearly parallel to the laser polarization. When the *c*-axis was perpendicular to the laser polarization, we also observe a decrease in intensity of the higher frequency component, and by ~10 GPa the emission band is asymmetrical but both components can still be deconvolved. It is possible that the merging of the peaks reported by Mernagh and Liu (1991) and Parthasarathy (1997) is the result of changes in sample orientation between pressure steps.

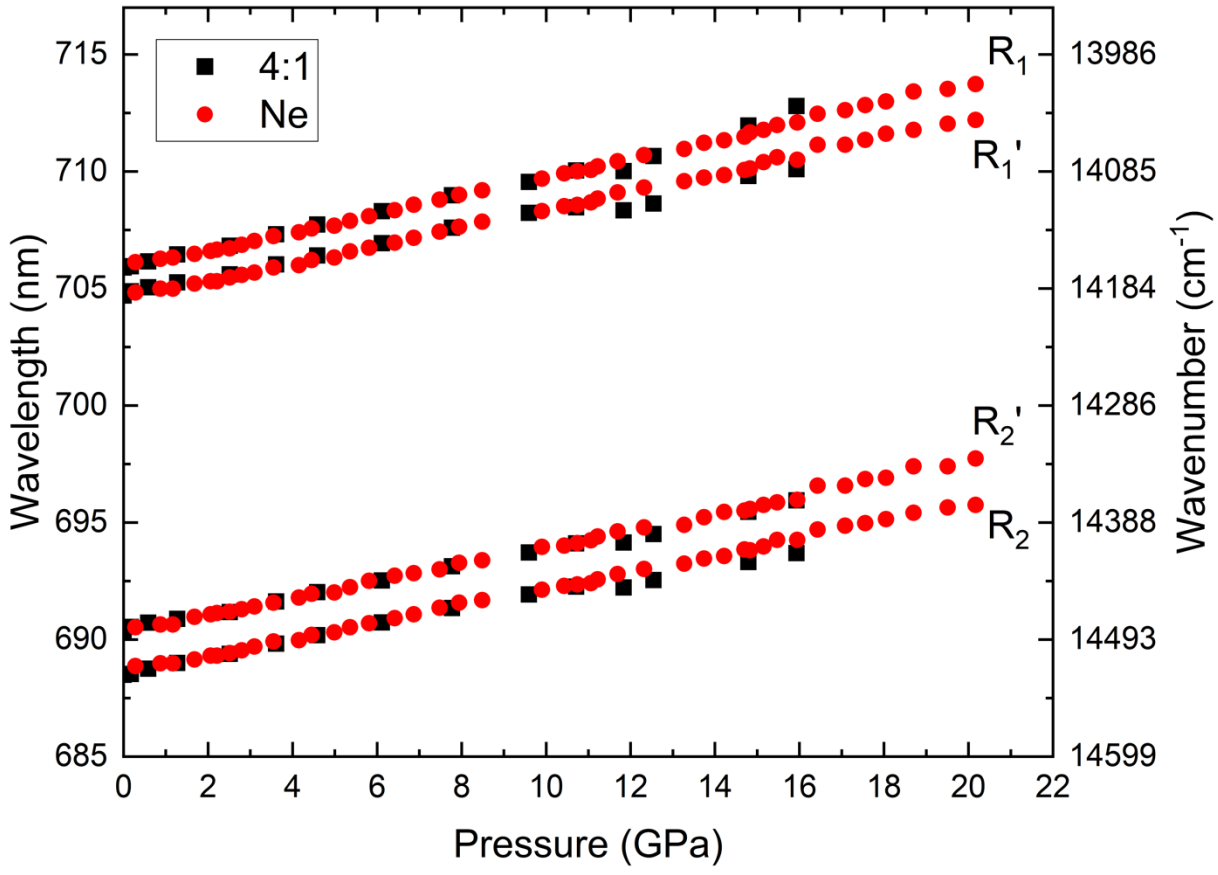

Figure 10. R-line peak positions of kyanite as a function of pressure from two runs; one in a 4:1 PTM and one in a Ne PTM. R_1 and R_2 are associated with the M1 site, and R_1' and R_2' are from the M2 site.

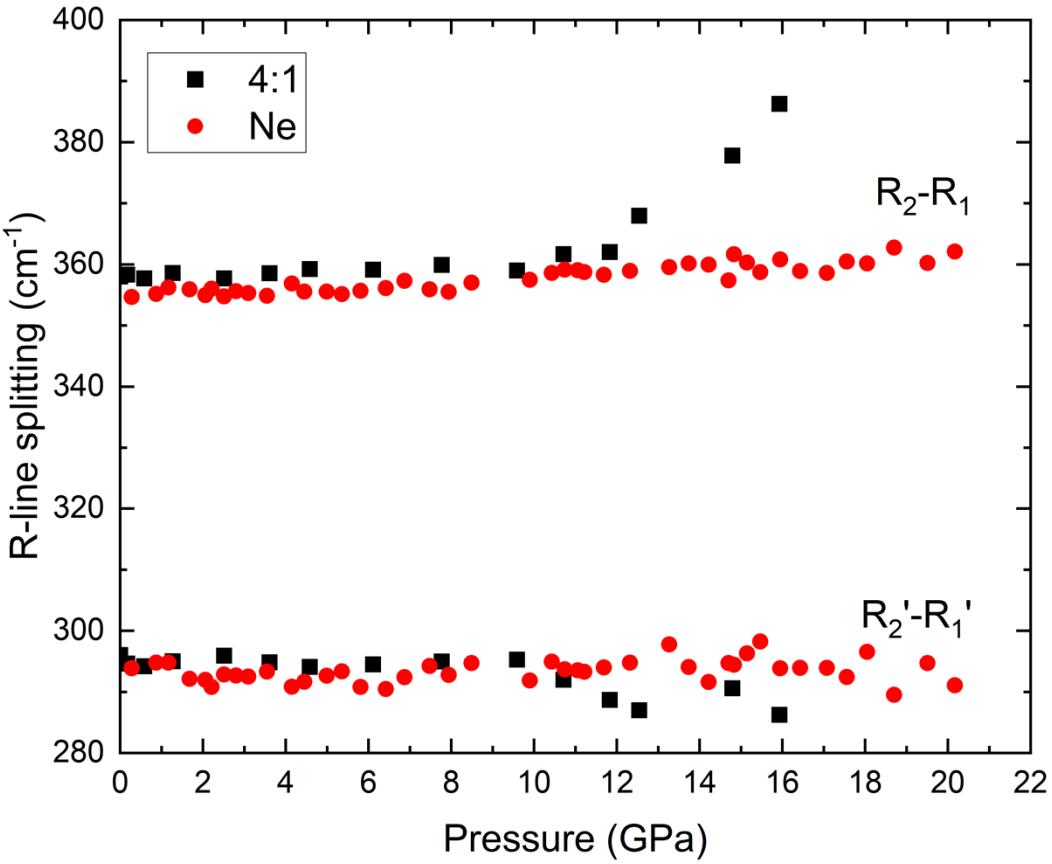

Figure 11. R-line splitting as a function of pressure. For the sample compressed in a 4:1 PTM, the R-line splitting from the M1 site begins to increase above ~10 GPa, and the M2 site shows a slight decrease above 10 GPa. For the sample compressed in a Ne PTM, the R-line splitting changes minimally for both sites up to ~20 GPa.

Recently, a phase transition was reported to occur at 9.7 GPa in kyanite (Gao et al., 2020). Gao et al. (2020) used either a KBr pressure medium or silicone oil pressure medium and collected both Raman and infrared spectra up to 18.6 GPa. They used the appearance of new peaks, discontinuous shifts in certain peaks and changes in the pressure-dependent slope of several peaks as evidence for a phase transition at ~9.7 GPa to a phase they termed kyanite-II. The present luminescence study, as well as previous vibrational and X-ray studies at room temperature and pressures up to 30 GPa, have not found evidence for any phase transitions in kyanite (Comodi et al., 1997; Friedrich et al., 2004; Liu et al., 2009; Mernagh and Liu, 1991; Yang et al., 1997). In particular, Mernagh and Liu (1991) conducted Raman spectroscopy to 14 GPa; Liu et al. (2009) performed powder diffraction to 17.5 GPa, and Yagi et al. (1998)

460 to 10.2 GPa. Friedrich et al. (2004) presented evidence for the persistence of kyanite to 30 GPa, with the
461 possible onset of a high-pressure transition above 30 GPa based on powder X-ray diffraction results. Gao
462 et al. (2020) offer three possible explanations for this discrepancy: (1) different PTM, (2) better spectral
463 resolution than previous studies, and (3) differences in trace element concentrations. Gao et al. (2020)
464 used KBr and silicone oil as their pressure media; each of these media is characterized by non-hydrostatic
465 gradients at low pressure conditions, with KBr supporting pressure gradients at low pressure conditions,
466 and silicone oil showing signs of pressure gradients above ~2.5 GPa (Klotz et al., 2009). Therefore, it is
467 possible that non-hydrostatic conditions may be at the root of this discrepancy. Differences in spectral
468 resolution between Gao et al. (2020) and (Mernagh and Liu, 1991) may be a possibility with respect to
469 Raman results, but it does not explain the non-observance of this transition in high-pressure powder
470 diffraction studies (Friedrich et al., 2004; Liu et al., 2009). Lastly, Gao et al. (2020) postulate that the very
471 low Fe content of their sample can possibly explain the phase transition, but the sample used in this study
472 and the study of Yagi et al., (1998) both had low Fe concentrations, and no evidence of the proposed
473 transition at 9.7 GPa was observed in either study.

474 The role of non-hydrostatic stress in generating (or inducing) possible phase transitions is
475 complex. If the proposed 9.7 GPa transition reported by Gao et al. (2020) is generated by non-hydrostatic
476 stress, then an extreme scenario would involve bridging of kyanite within the diamond cell. This would
477 introduce a complex stress field characterized by a large uniaxial component. Indeed, Gao et al. (2020)
478 loaded inhomogeneous thickness samples in a KBr pressure medium for Raman mapping of the
479 coexistence of kyanite and the proposed kyanite-II phases, with the rationale being “to generate a larger
480 concentration of stress”. In one of our spectroscopic experiments, the kyanite sample bridged between
481 the anvils, and we observed several new emission bands within this sample alone. In this run, we
482 compressed the sample directly to ~11 GPa and collected a spectrum (Figure 12). The new emission bands
483 in this spectrum indicated that a subset of the Cr^{3+} ions were present within octahedral sites with different

484 distortions and volumes than the M1 and M2 sites. Within this bridged sample, we increased the pressure
485 to above 15 GPa and collected another spectrum where additional emission bands were observed,
486 indicating that the new stress field had further modified the Cr^{3+} environments. On decompression, by ~
487 9.0 GPa, the sample was no longer bridged. All the spectra collected at ~9.0 GPa and below (within a
488 hydrostatic regime) showed the typical set of emission bands assigned to M1 and M2.

489 Importantly, uniaxial stress has long been known to generate structural changes that can induce
490 splitting of fluorescence lines (Imbusch et al., 1965). For example, ruby luminescence spectra collected
491 with different uniaxial stress applied along the direction Θ= 61±2° and ω=8±2° showed splitting due to
492 separation of the Cr^{3+} ions into two σ-sublattices (Monteil et al., 1984). Since our sample was oriented in
493 the DAC when the sample bridged, the applied uniaxial stress was along the *a*-direction. Thus, while the
494 predominant non-hydrostatic stress would likely be close-to-uniaxial, the full stress tensor in a bridged,
495 oriented sample within a pressure medium is not expected to be simple. The key point here is that Figure
496 12 demonstrates that particularly extreme non-hydrostatic stress in kyanite can induce reversible
497 structural changes within the first nearest neighbor coordination sphere relative to normal kyanite. We
498 speculate that this reversible behavior under differential stress could be driven by a soft shear mode
499 within kyanite's elastic tensor: however, constraints on the individual elastic constants of kyanite at high
500 pressure do not exist.

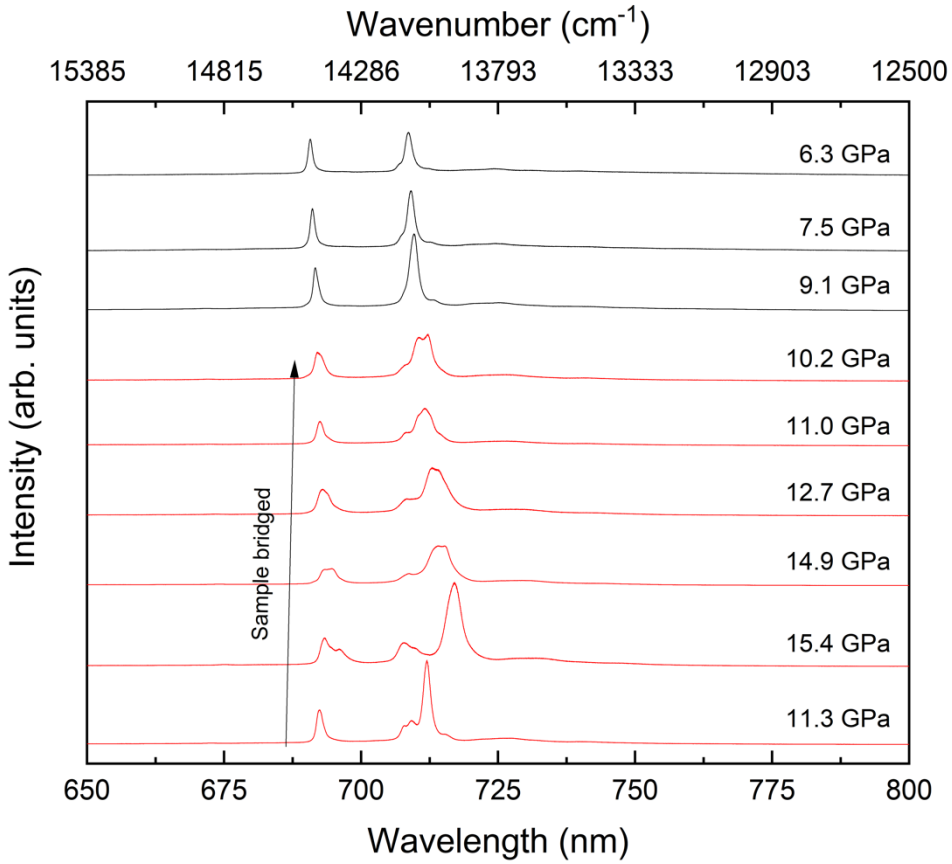

501

502 **Figure 12.** High pressure Cr^{3+} luminescence spectra of kyanite where the sample bridged between the
503 diamond anvils during the experiment. The red spectra (11.3 to ~10.2 GPa, bottom six spectra) were
504 collected while the sample was bridged. In the black spectra (9.1 to 6.3 GPa), the sample was no longer
505 bridged between the diamond anvils and the luminescence spectra show emission bands from only the
506 M1 and M2 sites.

507 **Conclusions**

508 The Cr^{3+} luminescence spectra of zoisite and kyanite have been characterized up to 40 and 20
509 GPa, respectively. These two minerals each have very large R-line splittings, and for zoisite the separation
510 increases as pressure increases and more than triples from its ambient value by 40 GPa. For comparison,
511 in kyanite the splitting remains virtually constant up to ~20 GPa when compressed in a Ne PTM. The
512 markedly different behavior of the Cr^{3+} substituted octahedral sites (the M3 site in zoisite and the M1 and
513 M2 sites in kyanite) indicate that the zoisite site increases dramatically in its distortion under pressure,
514 while the two sites in kyanite are largely unchanged: each of these results are in accord with substantially

lower pressure single-crystal diffraction results and demonstrate that R-line luminescence is a particularly sensitive probe of the octahedral metal sites. Notably, kyanite appears to be particularly sensitive to the onset of non-hydrostatic conditions. Phase transitions are not observed in either zoisite or kyanite up to the maximum pressure of each study, consistent with most previous studies. Lastly, we illustrate that the stress field of the sample is important for possible structural changes within kyanite, and that non-hydrostatic/nearly uniaxial stress components can produce anomalous luminescence and structural results in this material.

Acknowledgements

We thank Rob Franks for help with LA-ICPMS measurements, Dan Sampson for help with the Raman spectrometer, and two anonymous reviewers for helpful comments on the manuscript. A portion of this work was performed under the auspices of the US Department of Energy by Lawrence Livermore National Laboratory under Contract No. DE-AC52-07NA27344. Work partially supported by NSF through EAR-1620423 and EAR-2017294, and COMPRES under NSF Cooperative Agreement EAR 11-57758.

Author Contributions

E.F.O. prepared and carried out the experiments. E.F.O. carried out the data analysis with input from Q.W. E.F.O. and Q.W. wrote the manuscript.

Competing Interests

The authors declare no competing interests.

References

Ahmed-Zaid, I., and Madon, M. (1991) A high-pressure form of Al_2SiO_5 as a possible host of aluminum in the lower mantle. Nature, 353(6343), 426-428.

Alvaro, M., Angel, R.J., and Camara, F. (2012) High-pressure behavior of zoisite. American Mineralogist, 97(7), 1165-1176.

Arlt, T., and Angel, R.J. (2000) Displacive phase transitions in C-centred clinopyroxenes: spodumene, $LiScSi_2O_6$ and $ZnSiO_3$. Physics and Chemistry of Minerals, 27(10), 719-731.

Armbruster, T., Bonazzi, P., Akasaka, M., Bermanec, V., Chopin, C., Giere, R., Heuss-Assbichler, S., Liebscher, A., Menchetti, S., Pan, Y., and Pasero, M. (2006) Recommended nomenclature of epidote-group minerals. European Journal of Mineralogy, 18(5), 551-567.

Bartram, R.H., and Stoneham, A.M. (1975) Luminescence and abscence of luminescence of *F* centers. Solid State Communications, 17(12), 1593-1598.

Burnham, C.W. (1963) Refinement of the crystal structure of kyanite. Zeitschrift Fur Kristallographie, 118, 337-360.

Burns, R. (1993) Mineralogical applications of crystal field theory. Cambridge University Press.

Camara, F., Gatta, G.D., Meven, M., and Pasqual, D. (2012) Thermal expansion and high temperature structure evolution of zoisite by single-crystal X-ray and neutron diffraction. Physics and Chemistry of Minerals, 39(1), 27-45.

Chai, M., and Brown, J.M. (1996) Effects of static non-hydrostatic stress on the R lines of ruby single crystals. Geophysical Research Letters, 23(24), 3539-3542.

Chervin, J.C., Canny, B., and Mancinelli, M. (2001) Ruby-spheres as pressure gauge for optically transparent high pressure cells. International Journal of High Pressure Research, 21(6), 305-314.

Chopelas, A., and Nicol, M. (1982) Pressure dependece to 100 kilobars of the phonons of MgO at 90 K and 295 K. Journal of Geophysical Research, 87(NB10), 8591-8597.

Comodi, P., and Zanazzi, P.F. (1997) The pressure behavior of clinozoisite and zoisite: An X-ray diffraction study. American Mineralogist, 82(1-2), 61-68.

Comodi, P., Zanazzi, P.F., Poli, S., and Schmidt, M.W. (1997) High-pressure behavior of kyanite: Compressibility and structural deformations. American Mineralogist, 82(5-6), 452-459.

Czaja, M., Marzurak, Z., and Lukowiak, E. (1995) Spectroscopic properties and crystal-field analysis of Cr^{3+} ions in kyanite Al_2SiO_5. Journal of Applied Spectroscopy, 62(4), 648-655.

d'Amour, H., Schiferl, D., Denner, W., Schulz, H., and Holzapfel, W.B. (1978) High-pressure single-crystal structure determinations for ruby up to 90 kbar using an automatic diffractometer. Journal of Applied Physics, 49(8), 4411-4416.

Dewaele, A., Torrent, M., Loubeyre, P., and Mezouar, M. (2008) Compression curves of transition metals in the Mbar range: Experiments and projector augmented-wave calculations. Physical Review B, 78(10).

Dobrzhinetskaya, L.F., and Green, H.W. (2007) Experimental studies of mineralogical assemblages of metasedimentary rocks at Earth's mantle transition zone conditions. Journal of Metamorphic Geology, 25(2), 83-96.

Dollase, W.A. (1968) Refinement and comparison of structures of zoisite and clinozoiste. American Mineralogist, 53(11-1), 1882-&.

-. (1969) Crystal structure and cation ordering of piemontite. American Mineralogist, 54(5-6), 710-&.

-. (1971) Refinement of the crystal structures of epidote, allanite, and hancockite. American Mineralogist, 56(3-4), 447-&.

-. (1973) Mossbaur spectra and iron distribution in epidote-group minerals. Zeitschrift Fur Kristallographie, 138, 41-63.

579 Finger, L.W., and Hazen, R.M. (1978) Crystal-structure and compression of ruby to 46 kbar. Journal of
580 Applied Physics, 49(12), 5823-5826.
581 Forneris, J.F., and Holloway, J.R. (2003) Phase equilibria in subducting basaltic crust: implications for H_2O
582 release from the slab. Earth and Planetary Science Letters, 214(1-2), 187-201.
583 -. (2004) Evolution of mineral compositions during eclogitization of subducting basaltic crust. American
584 Mineralogist, 89(10), 1516-1524.
585 Fresenko, E.G., Rumanova, I.M., and Belov, N.V. (1955) The crystal structure of zoiste. Dokl. Acad. Sci.
586 USSR, 102, 275-278.
587 Friedrich, A., Kunz, M., Winkler, B., and Le Bihan, T. (2004) High-pressure behavior of sillimanite and
588 kyanite: compressibility, decomposition and indications of a new high-pressure phase.
589 Zeitschrift Fur Kristallographie, 219(6), 324-329.
590 Gaft, M., Nagli, L., Panczer, G., & Rossman, G. (2013). Long-lived laser induced time-resolved
591 luminescence of Cr^{3+} in kyanite Al_2SiO_5. Journal of Spectroscopy and Dynamics, 3, 22-29.
592 Gaft, M., Reisfeld, R., and Panczer, G. (2015) Modern luminescece spectroscopy of minerals and
593 materials. Springer.
594 Gao, J., Wu, W.H., Jia, L.H., Wang, C.P., Liu, Y.X., Xu, C.W., Chen, F., Fei, C.H., and Su, W. (2020) Raman
595 and infrared spectra to monitor the phase transition of natural kyanite under static
596 compression. Journal of Raman Spectroscopy, 51(10), 2102-2111.
597 Ghose, S., and Tsang, T. (1971) Ordering of V^{2+}, Mn^{2+} and Fe^{3+} ions in zoisite $Ca_2Al_3Si_3O_{12}(OH)$. Science,
598 171(3969), 374-&.
599 Grapes, R.H. (1981) Chromian epidote and zoisite in kyanite amphibolite, Southern Alps, New Zealand.
600 American Mineralogist, 66(9-10), 974-975.
601 Gupta, Y.M., and Shen, X.A. (1991) Potential use of the ruby R_2 line shift for static high-pressure
602 calibration. Applied Physics Letters, 58(6), 583-585.
603 Hazen, R.M., Au, A.Y., and Finger, L.W. (1986) High-pressure crystal chemistry of beryl ($Be_3Al_2Si_6O_{18}$) and
604 euclase ($BeAlSiO_4OH$). American Mineralogist, 71(7-8), 977-984.
605 Hejny, C., Konzett, J., Pippinger, T., Klotz, T., and Miletich, R. (2019) Pressure-enforced Cr substitution in
606 $Cr_{1+x}Al_{1-x}O(SiO_4)$, synthetic analogues of kyanite. Physics and Chemistry of Minerals, 46, 583-594.
607 Hua, H., Ueda, J., Xu, J., Back, M., and Tanabe, S. (2021) High-Pressure Photoluminescence Properties of
608 Cr^{3+}-Doped $LaGaO_3$ Perovskites Modulated by Pressure-Induced Phase Transition. Inorganic
609 Chemistry.
610 Hutton, D.R., and Troup, G.J. (1964) Paramagnetic resonance of Cr^{3+} in kyanite. British Journal of Applied
611 Physics, 15(3), 275-&.
612 Imbusch, G.F., Schawlow, A.L., May, A.D., and Sugano, S. (1965) Fluorescence of MgO: Cr^{3+} ions in
613 noncubic sites. Physical Review, 140(3A), A830.
614 Ito, T.I. (1950) X-ray studies on polymorphism. Maruzen Company, Limited.
615 Jahren, A.H., Kruger, M.B., and Jeanloz, R. (1992) Alexandrite as a high-temperature pressure calibrant,
616 and implications for the ruby pressure scale. Journal of Applied Physics, 71(4), 1579-1582.
617 Jenei, Zs., Cynn, H., Visbeck, K., and Evans, W.J. (2013) High-temperature experiments using a resistively
618 heated high-pressure membrane diamond anvil cell. Review of Scientific Instruments, 84(9).
619 Jovanic, B.R. (2000) Effect of high pressure on fluorescence lifetime and position for R1 line in synthetic
620 spinel $MgAl_2O_4 : Cr^{3+}$. In D.P. Uskokovic, G.A. Battiston, J.M. Nedeljkovic, S.K. Milonjic, and D.I.
621 Rakovic, Eds. Trends in Advanced Materials and Processes, 352, p. 247-250.
622 Klotz, S., Chervin, J.C., Munsch, P., and Le Marchand, G. (2009) Hydrostatic limits of 11 pressure
623 transmitting media. Journal of Physics D-Applied Physics, 42(7).
624 Kottke, T., and Williams, F. (1983) Pressure dependence of the alexandrite emission spectrum. Physical
625 Review B, 28(4), 1923-1927.

626 Koziarska, B., Godlewski, M., Suchocki, A., Czaja, M., and Mazurak, Z. (1994) Optical properties of zoisite.
627 Physical Review B, 50(17), 12297-12300.
628 Langer, K., and Seifert, F. (1971) High Pressure - High Temperature - Synthesis and properties of
629 chromium kyanite, $(Al,Cr)_2SiO_5$. Zeitschrift Fur Anorganische Und Allgemeine Chemie, 383(1), 29-
630 &.
631 Liu, X., Shieh, S.R., Fleet, M.E., and Zhang, L. (2009) Compressibility of a natural kyanite to 17.5 GPa.
632 Progress in Natural Science, 19(10), 1281-1286.
633 Mao, H.K., Xu, J., and Bell, P.M. (1986) Calibration of the ruby pressure gauge to 800 kbar under quasi-
634 hydrostatic conditions. Journal of Geophysical Research-Solid Earth and Planets, 91(B5), 4673-
635 4676.
636 Mernagh, T.P., and Liu, L.G. (1991) Raman spectra from the Al_2SiO_5 polymorphs at high pressures and
637 room temperature. Physics and Chemistry of Minerals, 18(2), 126-130.
638 Merrill, L., and Bassett, W.A. (1974) Minature diamond anvil cell for single-crystal X-ray diffraction
639 studies. Review of Scientific Instruments, 45(2), 290-294.
640 Mills, S.J., Hatert, F., Nickel, E.H., and Ferraris, G. (2009) The standardisation of mineral group
641 hierarchies: application to recent nomenclature proposals. European Journal of Mineralogy,
642 21(5), 1073-1080.
643 Monteil, A., Duval, E., Attar, A., Viliani, G., and Lacroix, R. (1984) Splitting of the ruby fluorescence under
644 stress. Journal De Physique Lettres, 45(22), 1097-1101.
645 Nagashima, M., Geiger, C.A., and Akasaka, M. (2009) A crystal-chemical investigation of clinozoisite
646 synthesized along the join $Ca_2Al_3Si_3O_{12}(OH)$-$Ca_2Al_2CrSi_3O_{12}(OH)$. American Mineralogist, 94,
647 1351-1360.
648 Naray-Szabo, S., Taylor, W.H., and Jackson, W.W. (1929) The structure of kyanite. Zeitschrift Fur
649 Kristallographie, 71, 117-130.
650 Nicholls, L.A., and Ringwood, A.E. (1973) Effect of water on olivine stability in tholeiites and production
651 of silica-saturated magmas in island-arc environment. Journal of Geology, 81(3), 285-300.
652 O'Bannon, E., III, Beavers, C.M., Kunz, M., and Williams, Q. (2018) High-pressure study of dravite
653 tourmaline: Insights into the accommodating nature of the tourmaline structure. American
654 Mineralogist, 103(10), 1622-1633.
655 O'Bannon, E., III, and Williams, Q. (2016a) Beryl-II, a high-pressure phase of beryl: Raman and
656 luminescence spectroscopy to 16.4 GPa. Physics and Chemistry of Minerals, 43(9), 671-687.
657 -. (2016b) A Cr^{3+} luminescence study of spodumene at high pressures: Effects of site geometry, a phase
658 transition, and a level-crossing. American Mineralogist, 101(5-6), 1406-1413.
659 -. (2017) Delocalization in Cr^{3+} luminescence of clinochlore: A pressure-induced transition from single-
660 ion emission to pair emission. Journal of Physics and Chemistry of Solids, 109, 89-99.
661 O'Bannon, E.F., III, and Williams, Q. (2019) A Cr^{3+} luminescence study of natural topaz $Al_2SiO_4(F,OH)_2$ up
662 to 60 GPa. American Mineralogist, 104(11), 1656-1662.
663 Ono, S. (1998) Stability limits of hydrous minerals in sediment and mid-ocean ridge basalt compositions:
664 Implications for water transport in subduction zones. Journal of Geophysical Research-Solid
665 Earth, 103(B8), 18253-18267.
666 Ono, S., Nakajima, Y., and Funakoshi, K. (2007) In situ observation of the decomposition of kyanite at
667 high pressures and high temperatures. American Mineralogist, 92(10), 1624-1629.
668 Parthasarathy, G. (1997) High-pressure behaviour of chromium ion as a fluorescing cation in Earth
669 materials. Advances in High Pressure Science and Technology: Proceedings of the Fourth
670 National Confernece on High Pressure Science and Technology. University Press, Indira Gandhi
671 Center for Atomic Research, Kalpakkam.
672 Peacock, S.M. (1990) Fluid processes in subduction zones. Science, 248(4953), 329-337.

673 Platonov, A.N., Tarashchan, A.N., Langer, K., Andrut, M., Partzsch, G., and Matsyuk, S.S. (1998) Electronic
674 absorption and luminescence spectroscopic studies of kyanite single crystals: differentiation
675 between excitation of FeTi charge transfer and Cr^{3+} dd transitions. Physics and Chemistry of
676 Minerals, 25(3), 203-212.
677 Poli, S., and Schmidt, M.W. (1998) The high-pressure stability of zoisite and phase relationships of
678 zoisite-bearing assemblages. Contributions to Mineralogy and Petrology, 130(2), 162-175.
679 Robinson, K., Gibbs, G.V., and Ribbe, P.H. (1971) Quadratic elongation: A quantitative measure of
680 distortion in coordination polyhedra. Science, 172(3983), 567-&.
681 Schmidt, M.W., and Poli, S. (1994) The stability of lawsonite and zoisite at high-pressures: Experiments
682 in CASH to 92 kbar and implications for the presence of hydrous phases in subducted
683 lithosphere. Earth and Planetary Science Letters, 124(1-4), 105-118.
684 Schmidt, M.W., Poli, S., Comodi, P., and Zanazzi, P.F. (1997) High-pressure behavior of kyanite:
685 Decomposition of kyanite into stishovite and corundum. American Mineralogist, 82(5-6), 460-
686 466.
687 Smith, J.V., Pluth, J.J., Richardson, J.W., and Kvick, A. (1987) Neutron diffraction study of zoisite at 15 K
688 and X-ray study at room temperature. Zeitschrift Fur Kristallographie, 179(1-4), 305-321.
689 Syassen, K. (2008) Ruby under pressure. High Pressure Research, 28(2), 75-126.
690 Tanabe, Y., and Sugano, S. (1954) On the absorption spectra of complex ions I. Journal of the Physical
691 Society of Japan, 9(5), 753-766.
692 Wamsley, P.R., and Bray, K.L. (1994) The effect of pressure on the luminescece of Cr^{3+} - YAG. Journal of
693 Luminescence, 59(1-2), 11-17.
694 Weinstein, B.A. (1986) Ruby thermometer for cryobaric diamond anvil cell. Review of Scientific
695 Instruments, 57(5), 910-913.
696 Welch, M.D., and Marshall, W.G. (2001) High-pressure behavior of clinochlore. American Mineralogist,
697 86(11-12), 1380-1386.
698 Wildner, M., Beran, A., and Koller, F. (2013) Spectroscopic characterisation and crystal field calculations
699 of varicoloured kyanites from Loliondo, Tanzania. Mineralogy and Petrology, 107(2), 289-310.
700 Winkler, B., Langer, K., and Johannsen, P.G. (1989) The influence of pressure on the OH valence
701 vibration of zoisite: An infrared spectroscopic study. Physics and Chemistry of Minerals, 16(7),
702 668-671.
703 Wojtowicz, A.J. (1991) Luminescence of Cr^{3+} in kyanite. Journal of Luminescence, 50(4), 221-230.
704 Xu, J., Zhang, D., Fan, D., Wu, X., Shi, F., and Zhou, W. (2019) Compressional behavior of natural eclogitic
705 zoisite by synchrotron X-ray single-crystal diffraction to 34 GPa. Physics and Chemistry of
706 Minerals, 46(4), 333-341.
707 Yagi, T., Inutsuka, S., and Kondo, T. (1998) Isothermal compression curve of Al_2SiO_5 kyanite. 5th US/Japan
708 Seminar on High Pressure-Temperature Research - Properties of Earth and Planetary Materials,
709 101, p. 281-286, Maui, Hi.
710 Yang, H.X., Downs, R.T., Finger, L.W., Hazen, R.M., and Prewitt, C.T. (1997) Compressibility and crystal
711 structure of kyanite, Al_2SiO_5, at high pressure. American Mineralogist, 82(5-6), 467-474.
712 Yeung, Y.Y., Qin, J., Chang, Y.M., and Rudowicz, C. (1994) Correlation of spectroscopic properties and
713 subsitutional sites of Cr^{3+} in aluminosilicates: I. Kyanite. Physics and Chemistry of Minerals,
714 21(8), 526-531.
715 Zhou, Y., Irifune, T., and Kuribayashi, T. (2021) Phase relations of the Al_2O_3-SiO_2 system at 13-21 GPa and
716 2300-2800 K and a new high-pressure $Al_2Si_2O_7$ phase. Physics and Chemistry of Minerals, 48(7).
717 Zhou, Y., Irifune, T., Ohfuji, H., and Kuribayashi, T. (2018) New high-pressure forms of Al_2SiO_5.
718 Geophysical Research Letters, 45(16), 8167-8172.

719

720